Composites Science and Technology 137 (2016) 78–86

Contents lists available at ScienceDirect

Composites Science and Technology

journal homepage: http://www.elsevier.com/locate/compscitech

Robust, self-healing, superhydrophobic coatings highlighted by a novel branched thiol-ene fluorinated siloxane nanocomposites

Hao Zhang, Yong Ma, Jiaojun Tan, Xinlong Fan, Yibin Liu, Junwei Gu, Baoliang Zhang, Hepeng Zhang, Qiuyu Zhang*

Key Laboratory of Applied Physics and Chemistry in Space of Ministry of Education, School of Science, Northwestern Polytechnical University, Xi'an 710072, PR China

ARTICLE INFO

Article history:
Received 1 August 2016
Received in revised form
27 October 2016
Accepted 28 October 2016
Available online 31 October 2016

Keywords:
Superhydrophobic
Thiol-ene
Interpenetrating polymer networks (IPN)
Self-healing

ABSTRACT

In this work, we present one-step dip-coating strategy for fabricating robust, self-healing and superhydrophobic coatings using a coating solution that contains a novel branched thiol-ene fluorinated siloxane (T-FAS), polydimethylsiloxane (PDMS) elastomer and hydrophobic fumed silica nanoparticles (SiO_2 NPs). The novel branched T-FAS, with low fluorinated surface energy and high sol-gel reactivity, was prepared by introducing (*N*-methyl-perfluorohexane-1-sulfonamide) ethyl acrylate (FSA) and γ-methacryloxypropyltrimethoxysilane (MPS) into pentaerythritol tetra (3-mercaptopropionate) (PETMP) via thiol-ene click reaction. The superhydrophobic coating, being high stable to strong acid, UV, thermal and smudge treatment, has a water contact angle of 165 ± 2° and shedding angle of 4 ± 1°. It can withstand at least 100 cycles of abrasion with 1500 grit sandpaper under 45 KPa due to the interpenetrating polymer networks (IPN) constructed by T-FAS/PDMS. The IPN is also self-healing to chemically etching using long perfluoro-terminated chains of T-FAS which can spontaneously reorient to new air interfaces. The robust self-healing IPN may lead to the development of new efficient strategies for durable protective coatings in various applications.

1. Introduction

Superhydrophobic surface that displays contact angle (CA) above 150° and contact angle hysteresis (CAH) below 10° shows excellent water repellency [1–3]. The emerging applications such as self-cleaning [4], anti-icing [5], anti-bacterial [6], drag-reduction [7], water/oil separation [8], energy conversion and storage [9], have attracted much attention in both scientific and industrial areas. And the superhydrophobic and self-healing coatings that could repel toxic and corrosive liquids are highly desirable [10].

Two essential protocols of superhydrophobic surfaces, low surface energy and multiscale surface roughness, were first confirmed [11,12]. Recently, great progresses including etching [13,14], lithography [15], electrodeposition [16], physical/chemical vapor deposition [17,18], electrospinning [19], self-assembly [20], template synthesis [21], sol-gel process [22], and hot-pressing method [23] have been made in preparing superhydrophobic surfaces, however, some challenges still remain to overcome in technologies to coatings.

The major issue that needs to be confronted is the durability [24,25].As a result of the fragility of the micro/nano-scopic roughness features that are necessary for superhydrophobicity, most superhydrophobic surfaces are low in mechanical robustness [26]. To improve the durability, several strategies have been developed, such as crosslinking [27,28], self-healing [29–31] or hierarchical roughening [21,30]. Beside, nanoparticles and fibers (e.g., SiO_2, ZnO, TiO_2 and CNT) are often applied to the superhydrophobic coating preparation, which drastically improve wear resistance and water repellency [22,32–35]. Typically, Lin's group used crosslinked Polydimethylsiloxane (PDMS) filled with fluorinated alkyl silane (FAS) functionalised silica nanoparticles and FAS to prepare highly durable superhydrophobic fabrics. After 28 000 cycles of Martindale abrasion with wool felt under 12 KPa, the water contact angle (WCA) still showed above 150° and the nanoscale roughness could still be observed [36]. They also reported a self-healing superamphiphobic fabric coating that was prepared from hydrolyzed fluoroalkyl silane (FAS) containing well-dispersed fluorinated-decyl polyhedral oligomeric silsequioxane (FD-POSS) [37].

* Corresponding author.
E-mail address: qyzhang@nwpu.edu.cn (Q. Zhang).

http://dx.doi.org/10.1016/j.compscitech.2016.10.023
0266-3538/

Another important challenge is a rapid, highly efficient fabrication [38–40]. It is a remarkable fact that sol-gel and click chemistry representing rapid, highly efficient methods have marked a major escalation in applications [41,42]. Recently, Li et al. presented a simple strategy for fabricating of superamphiphobic coatings using spray-deposition and UV photopolymerization of thiol-ene resins that contained hydrophobic silica nanoparticles and perfluorinated thiols. The WCA remained above 150° after 200 abrasion cycles with 2000 grit sandpaper under 0.25 KPa [40].

Herein, to fix these problems, a superhydrophobic fabric after being dip-coated with polydimethylsiloxane (PDMS), novel branched fluorinated siloxane (T-FAS) and hydrophobic fumed silica nanoparticles (SiO_2 NPs) was reported. The novel branched T-FAS was prepared by introducing (*N*-methyl-perfluorohexane-1-sulfonamide) ethyl acrylate (FSA) and γ-methacryloxypropyltrimethoxysilane (MPS) into pentaerythritol tetra (3-mercaptopropionate) (PETMP) via thiol-ene click reaction. The branched T-FAS uses an average of two long fluoroalkyl chains as self-healing superhydrophobic arms and hydrolysable silane chains as durable bodies, respectively, being more reactive and flexible than FAS meanwhile practical than thiol-ene photopolymerization. When exposed to air, the rapidly hydrolysable T-FAS combines PDMS and SiO_2 NPs into the IPN which displays remarkable durability against severe abrasion damages. Two other long perfluoro-terminated chains via T-FAS overall connected to the networks can spontaneously reorient to new air interfaces for self-healing superhydrophobicity against chemically etching. Most notable among these should be the highly durable crosslinking IPN with self-healing properties.

2. Experimental

2.1. Materials

Perfluorinated (*N*-methyl-perfluorohexane-1-sulfonamide) ethyl acrylate (FSA, > 95%) was provided by Hengxin chemical Co. (Hubei) and recrystallization in methanol. Pentaerythritol tetra (3-mercaptopropionate) (PETMP) used as received was obtained from Evans Chemetics. γ-methacryloxypropyltrimethoxysilane (MPS, > 98%) and dimethyl phenyl phosphine (DMPPH) were purchased from Aldrich. PDMS Sylgard 184 (Dow Corning Corporation) was supplied as a two-part kit consisting of prepolymer (base, Sylgard 184 -A) and crosslinker (curing agent, Sylgard 184 - B) components. Traditionally, the prepolymer and crosslinker are mixed at 10: 1 weight ratio. Hydrophobic fumed silica nanoparticles (Aerosil R972), with an average primary particle size of 16 nm, was obtained by Evonik Industries. Other reagents and organic solvents from J&K Scientific Co. were used without any further purification unless otherwise specified. Commercial fabrics (65% polyester, 35% cotton) were purchased from local supermarket, and rinsed with ethanol and distilled water.

2.2. Preparation of FSA/MPS modified thiols

The novel branched T-FAS was synthesized using a phosphine-catalyzed nucleophilic thiol Michael addition reaction to acrylates following a synthetic process established by Shin's groups [43]. PETMP was first mixed with 0.1 wt % of DMPPH in anhydrous acetone while nitrogen purging. FSA/MPS at 1:1 M ratios was dripped into the mixture for 10 min and the temperature was controlled below 30 °C in order to prevent acrylates from undergoing thermally-initiated free-radical polymerization. 1: 2 M ratios between PETMP and FSA/MPS were used for the modified quaternary systems (solution concentration: 50 wt %). After adding FSA/MPS, the mixture was further reacted for 3 h at room temperature until all acrylates were consumed.

2.3. Preparation of self-healing, superhydrophobic coatings solution

The T-FAS, PDMS prepolymer Part-A (base, Sylgard 184 -A) and SiO_2 NPs were added to tetrahydrofuran (THF). The solution was ultrasonicated for 1 h to be the Solution A. PDMS precursor Part-B (curing agent, Sylgard 184 -B) was dissolved in THF to be the Solution B. The prepolymer and crosslinker are figured out at 10: 1 weight ratio.

2.4. Preparation of self-healing, superhydrophobic coatings

Prior to coating treatment, the Solutions A and B were mixed together at room temperature to form a coating solution. Fabric samples were dip-coated with the as-prepared coating solution and then cured at 135 °C for 30 min.

2.5. Characterization

2.5.1. Abrasion durability

The abrasion resistance was related to the modified AATCCA Test Method 8-2001. More specifically, the superhydrophobic fabric that kept contact with the sandpaper (1500 mesh served as an abrasion interface) instead of wool felt was subjected to 45 KPa, and dragged in a reciprocating motion with a speed of 60 cycles/min and abrasion length of 10 cm, respectively.

2.5.2. Stress-strain and bending modulus tests

The fabrics were stress-strain tested according to the ASTM D5035 method using a universal mechanical testing machine, Instron model 3367, equipped with a load cell of 30 KN. The bending modulus of fabrics was measured according to the ASTM D1388 method using a stiffness tester, BS model 3356. Bending modulus (Q, g/cm^2) was calculated according to the equations

$$Q = \frac{12G \times 10^{-6}}{g^3}, \quad G = 0.1MC^3,$$

where C and g are bending length and fabric thickness, respectively. G is the flexural rigidity of the sample, and M is the areal density of the fabric.

2.5.3. Chemical etching and self-healing

The chemical etching and self-healing property were tested using strong acid (H_2SO_4, pH = 1) and base solutions (KOH, pH = 14) at room temperature for certain hours.

2.5.4. UV, thermal and anti-smudge durability

The samples were exposed to UV light for 48 h at room temperature to assess the UV-durability of the modified coatings. An artificial UV source (100 W) emitting a spectrum which peaked at 365 nm was used for irradiations.

The coated fabrics were selected to carry out thermal durability test in an air-circulating oven at 150 °C for 24 h.

Maxwell coffee solution (a bag of 13 g dissolved in 150 ml water) was used as model of contamination to evaluate the anti-smudge ability of the superhydrophobic film.

2.5.5. Other characterizations

Fourier transform infrared (FT-IR) spectra were recorded using a TENSOR27 FTIR spectrometer (Bruker) between the frequency ranges of 4000–450 cm^{-1}. All 1H NMR spectra of T-FAS were operated by an INOVA - 400 spectrometer (Varian), using $CDCl_3$ as a solvent. Photoelectron spectroscopy (XPS) was obtained on a Kratos

AXIS Ultra DLD spectrometer at a 90 °C takeoff angle equipped with a 300 W monochromatic Al Kα X-Ray source. The binding energy values were referenced to the C1s line at 284.7 eV. The microstructure of the surface on the polyester-cotton fabric substrate was observed by scanning electron microscopy (SEM, JEOL JSM - 6700F).

The contact angle (CA) images were recorded on a Powereach JC2000D1 contact angle analyzer at room temperature. The shedding angle (SA), instead of sliding angle, was used according to a previous reported method [44]. To avoid the influence from droplet weight and size, CA and SA were measured using 8 μL and 35 μL liquid droplets. All the listed angles were determined by the average of 5 tests at least according to Laplace-Young fitting model.

3. Results and discussion

3.1. Synthesis and characterization of T-FAS

The preparation of the branched T-FAS is described in the Experimental section in details. Briefly, the tetra-functional thiol PETMP was modified with FSA and MPS in a nucleophile-initiated reaction via a thiol-ene click process yielding a novel T-FAS (Fig. 1a). Such thiol-ene click reaction that requires only 0.1 wt % DMPPH, can be easily performed under a normal air atmosphere, exhibit rapid and quantitative conversions (in a few seconds), and produce no side products. T-FAS possessing high-reactivity and low-energy includes A_0B_4, A_1B_3, A_2B_2, A_3B_1, A_4B_0 types that account for 6.25%, 25.0%, 37.5%, 25%, 6.25% by means of the probability theory and the mathematical statistics, respectively, according to the equations below:

$$P_{A_2B_2} = \frac{C_4^2}{C_4^0 + C_4^1 + C_4^2 + C_4^3 + C_4^4} \quad (1)$$

$$P_{A_1B_3} = \frac{C_4^1}{C_4^0 + C_4^1 + C_4^2 + C_4^3 + C_4^4} \quad (2)$$

$$P_{A_3B_1} = \frac{C_4^3}{C_4^0 + C_4^1 + C_4^2 + C_4^3 + C_4^4} \quad (3)$$

$$P_{A_4B_0} = \frac{C_4^4}{C_4^0 + C_4^1 + C_4^2 + C_4^3 + C_4^4} \quad (4)$$

$$P_{A_0B_4} = \frac{C_4^0}{C_4^0 + C_4^1 + C_4^2 + C_4^3 + C_4^4} \quad (5)$$

Here, FSA unit was termed as A, and MPS unit termed as B.

The chemical structures of functionalized T-FAS were confirmed by FT-IR and 1H NMR. Fig. 1b shows the typical FTIR spectra of the reactants (mixture of PETMP, FSA and MPS) and products (T-FAS). A strong peak assigned to Si-O asymmetric stretching vibrations was visible at 1100 cm^{-1} for all of the samples. Besides, peaks at 470 cm^{-1} and 800 cm^{-1} caused by Si-O rocking vibrations and Si-O bending vibrations, respectively, were also observed. In addition, the common peak at 1730 cm^{-1} resulting from C=O stretching vibrations of the ester groups, the peaks at 1210 cm^{-1} and 1100 cm^{-1}, corresponded to $-CF_2$ and $-SO_2-$ groups respectively, were visible. When T-FAS was achieved by a thiol-ene click process,

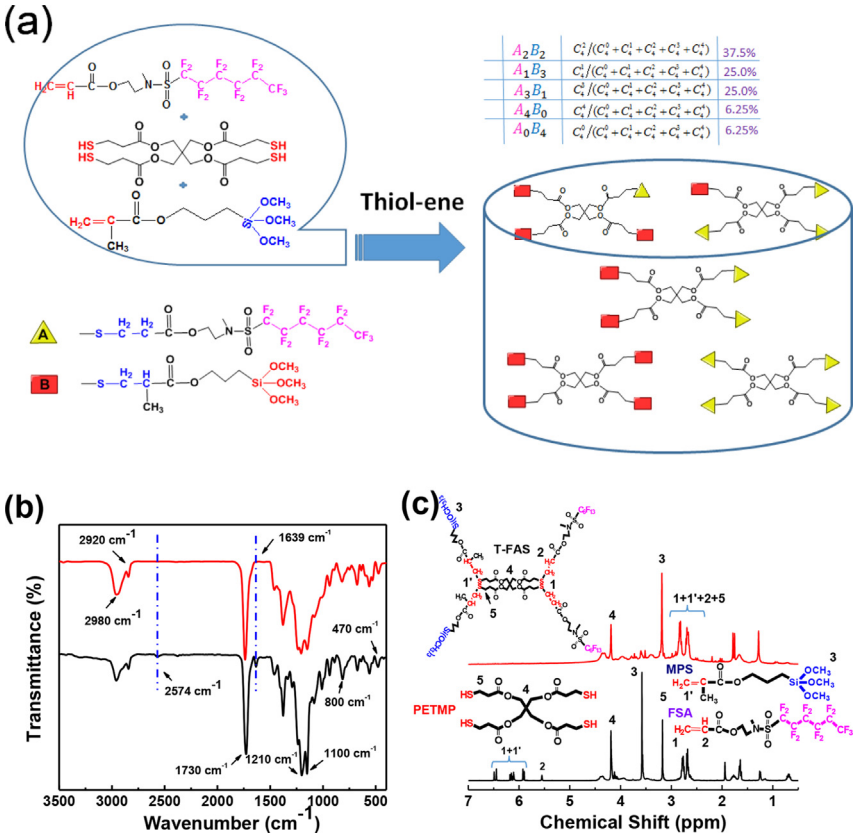

Fig. 1. (a) Schematic of the preparation for T-FAS via a thiol-ene click process, (b) FTIR spectra of the reactants (mixture of PETMP, FSA and MPS) and products (T-FAS), (c) 1H NMR spectra of the reactants (mixture of PETMP, FSA and MPS) and products (T-FAS).

the characteristic absorption band of thiol group at 2574 cm^{-1} and ene group at 1639 cm^{-1} disappeared. Furthermore, the relative absorption peak intensity at 2980 cm^{-1} and 2920 cm^{-1}, respectively, assigned to $-CH_3$ and $-CH_2$ stretching vibrations dramatically increase.

The typical 1H NMR spectra obtained from the reactants and products are shown in Fig. 1c. Several key features are evident. When comparing the 1H NMR spectrum in the reactants with products, it is clear that the resonances associated with the vinyl end-group, previously observed at 5.6–6.5 ppm, have completely disappeared while the relative broad peaks intensity at 2.4–2.7 ppm for T-FAS, corresponding to the methylene and methyne protons at the thioether linkage dramatically strengthen, which confirms the success of thiol-ene coupling PETMP with FSA and MPS. Besides, the methyl proton close to Si-O for FSA could be found at 3.6 ppm, which shifts quantitatively to 3.2 ppm. And the signals of the methylene protons adjacent to the thiol group at 3.2 ppm for the reactants, completely are replaced by 2.7 ppm but overlap with another the methylene and methyne resonance.

3.2. Film formulation and fabrication

Fig. 2a illustrates the chemical structures of the materials and the process to prepare the superhydrophobic coatings. The coating materials were formulated with a branched T-FAS, a PDMS pre-polymer/curing agent and SiO_2 NPs using a one-step dip-coating method. When exposed to air after coating treatment, the IPN was formed by highly hydrolysable crosslinked T-FAS and cured PDMS. And parts of the hydrolyzed T-FAS were coated on the SiO_2 NPs and substrate. The SiO_2 NPs with an average primary particle size of 16 nm serve the purpose of imparting a multiscale (micro/nano), or hierarchical morphology that is necessary to achieve superhydrophobic wetting properties on the cured coatings, following a Cassie-Baxter model (Fig. S1) [45].

3.3. Super-repellency behavior and mechanical durability

The super-repellency behavior of the coated films was evaluated by measuring CA and SA using both high- and low-surface-tension liquids, including water ($\gamma = 72.3$ mN/m), glycerol ($\gamma = 63.4$ mN/m) and ethylene glycol ($\gamma = 48.3$ mN/m). Fig. 2d–f systematically summarizes the wetting behavior and mechanical durability for the T-FAS:PDMS weight ratio (0: 100, 25: 75, 50: 50, 75: 25, and 100: 0) with a concentration of 4.0 wt % as well as the amount of SiO_2 NPs loading (0.5 wt %, 1.0 wt % and 1.5 wt % by weight relative to the total weight).

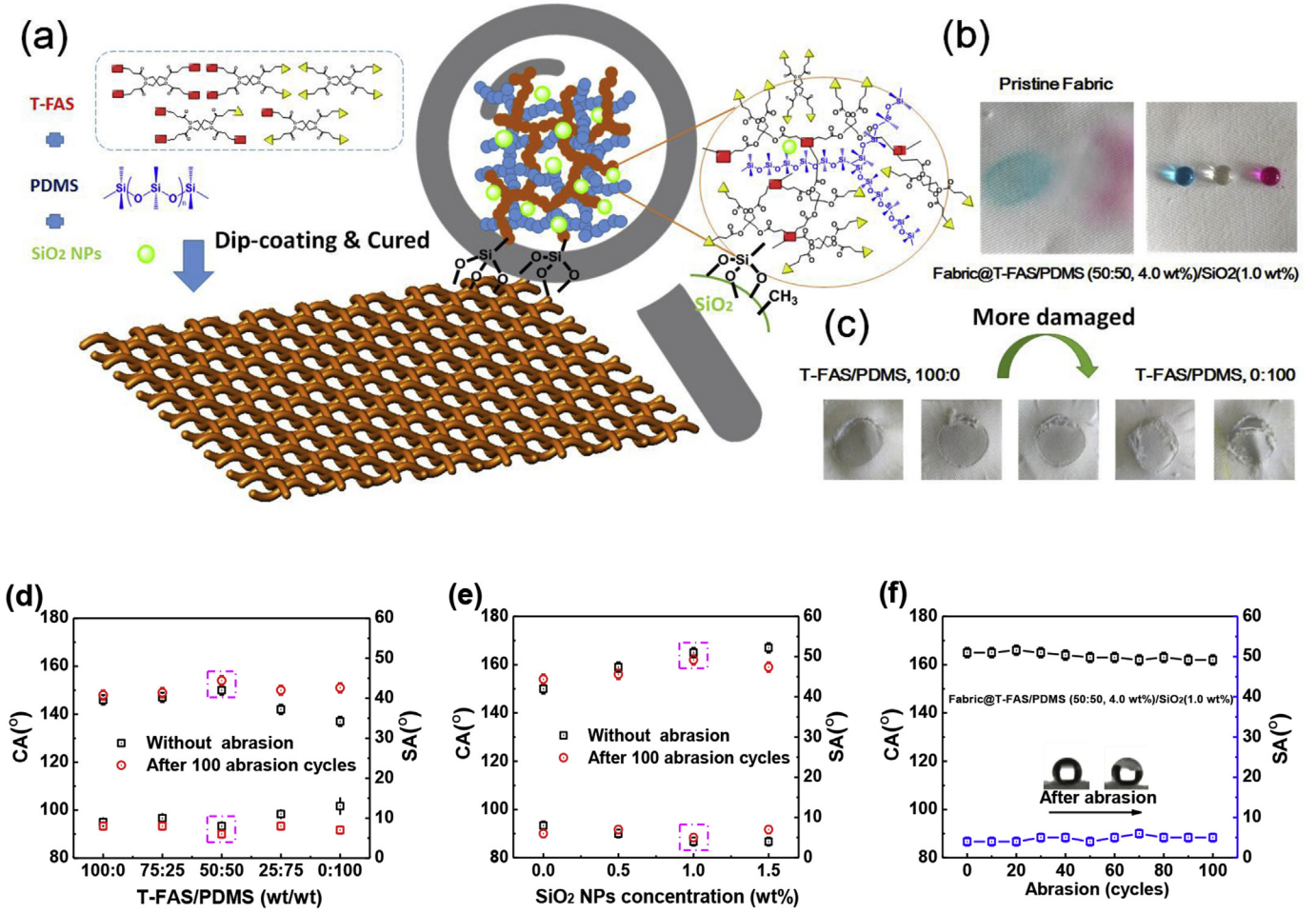

Fig. 2. (a) Procedure for coating treatment and IPN structure of T-FAS/PDMS, (b) photographs of blue-colored water, clear glycerol and red-colored ethylene glycol drops (35 μL) on the uncoated fabric and the coated fabric, (c) photographs of the coated fabrics with the different ratios of T-FAS/PDMS after 100 abrasion cycles, (d) Influences of T-FAS/PDMS in the coating solution on WCA and WSA after 100 abrasion cycles, (e) Influences of SiO_2 NPs concentration in the coating solution on WCA and WSA after 100 abrasion cycles, (f) WCA and WSA change with abrasion cycles for Fabric @T-FAS/PDMS (50: 50, 4.0 wt %)/SiO_2 (1.0 wt %). (For interpretation of the references to colour in this figure legend, the reader is referred to the web version of this article.)

The super-repellency to colored liquid droplets (35 μL) sitting on the coated fabric is showed in Fig. 2b. The spherical droplets of blue-colored water, clear glycerol and red-colored ethylene glycol have both superhydrophobic and oleophobic properties. The coated fabric showed CA of 165 ± 2°, 147 ± 2° and 142 ± 2° and SA of 4 ± 1°, 12 ± 2° and 15 ± 2° to water, glycerol and ethylene glycol, respectively. Moreover, the super-repellency behavior was stable to time as showed in Fig. S2. However, when blue-colored water, colorless glycerol and red-colored ethylene glycol were dropped on to the pristine fabric, the liquid completely spread into the fabric and no contact angle could be observed. The super-repellency behavior was also proved by the status in blue-colored water. The coated fabric was floated using the covering gas member on the fabric, following a Cassie-Baxter model, while the uncoated fabric sunk without protection (Fig. S3).

Focus is given to mechanical stability considering limitation in technological applications on the premise of superhydrophobicity. Fig. 2d–f record the changes of the water contact angle (WCA) and shedding angle (WSA) for films in different T-FAS/PDMS and SiO_2 NPs weight ratios after 100 abrasion cycles. Introducing T-FAS sharply increases hydrophobicity and durability. The CA changes little even though breakage occurs. And surprisingly, adding PDMS increases hydrophobicity during abrasion, with an increase in WCA and decrease in WSA. Such an unexpected increase in liquid repellency should be ascribed to the increased surface roughness due to abrasion. But it is achieved at a cost of durability. The fabrics, containing T-FAS especially below 25%, were seriously damaged (Fig. 2c). T-FAS and PDMS may act synergistically to attain durable superhydrophobicity. As expected, the maximum WCA and minimum WSA changed from 150 ± 2° and 8 ± 1° before abrasion to 154 ± 2° and 6 ± 1° after 100 abrasion cycles with the T-FAS/PDMS ratio at 50/50.

When adding SiO_2 NPs into the optimal T-FAS/PDMS films, the Super-repellency attains. Though the WCA decreased while WSA increased after abrasion, as the SiO_2 NPs weight ratio increased, WCA and WSA still remained above 150° and below 10°. The film of T-FAS/PDMS (50: 50, 4.0 wt %)/SiO_2 (1.0 wt %) showed optimal performance that WCA and WSA changed slightly from 165 ± 2° and 4 ± 1° before abrasion to 162 ± 2° and 5 ± 1° up to 100 abrasion cycles, making the liquids roll off rapidly from the coated fabric surface (Fig. 2f, Movie S1 & 2).

Supplementary video related to this article can be found at http://dx.doi.org/10.1016/j.compscitech.2016.10.023.

The fabric still remains above 150° derived from the interpenetrating polymer network (IPN). The IPN, using long perfluoro-terminated chains of branched T-FAS as arms, consists of highly cross-linked hydrolysable silane chains of T-FAS and PDMS, showing durable super-repellency. Besides, the hydrolysable silane of T-FAS interacts with the polar groups (e.g., hydroxyl group) of SiO_2 NPs and polyester like a coupling agent to enhance coating adhesion. The SiO_2 NPs incorporated in the network via covalent bonding restrict the deformation and increase hierarchical roughness of network (Fig. 4b), which reinforce the wear resistance and improve the liquid repellency illustrated in Fig. 2a.

The interaction derived from IPN also affect fiber mechanical and softening property. Fig. 3a and b records the typical stress-strain curve of fibers before and after coated. The fiber tensile strength at break increased from 617 ± 62 and 293 ± 25 MPa before coated to 714 ± 55 and 321 ± 20 MPa after coated, respectively, in the warp and weft. Fig. 3c shows the typical bending modulus change of fibers before and after coated. The bending modulus changes from 13.7 ± 1.5 and 11.5 ± 0.9 g/cm^2 before coated to 23.6 ± 2.5 and 17.2 ± 1.8 g/cm^2 after coated, respectively, in the warp and weft. Such an increase in the tensile properties should be attributed to the T-FAS/PDMS IPN and good bonding of the coating with the fiber substrate. The inset in Fig. 3a shows the fractured end of the coated fibers. The cracks could be seen on the fracture surface but the SiO_2 nanoparticles close to the section were still tightly attached to the surface. This illustrates that the coating layer could stick firmly on the fiber and fiber breaks before and after external deformation.

3.4. Surface morphology and chemical composition

The super-repellent behavior could be ascribe to the surface morphology and chemical composition. The morphological information of Pristine Fabric and Fabric @T-FAS/PDMS/SiO_2 were investigated by SEM, as shown in Fig. 4a and b. The microscale fibers of uncoated fabric (Fig. 4a) are smooth and round, exhibiting micro-scale roughness and consisting of twisted yarns with a diameter about 10 μm. Bumps are obviously observed on Fabric @T-FAS/PDMS compared by @T-FAS and @PDMS because of the difference of crosslinking shrinkage between T-FAS and PDMS, leading to high hydrophobicity (Fig. S4). Moreover, SiO_2 NPs enhanced roughness in conjunct with the micro-scale roughness inherent in the fabric is vital to obtain super-repellent fabrics (Fig. 4b). The decrease in WCA and increase in WSA upon abrasion can be attributed to damage to the hierarchical morphology, especially to nano-scale roughness of SiO_2 NPs, the damaged fibers were observed in Fig. 4c.

For further clarify the superhydrophobic mechanism of coated fabrics, their chemical components were verified by FTIR and XPS. Fig. 4d shows the changes in the typical FTIR spectra of Pristine Fabric and @T-FAS/PDMS/SiO_2. The strong peaks assigned to C=O and C-O vibration asymmetric stretching vibrations was visible at 1730 cm^{-1} and 1020 cm^{-1} for all of the samples. When fabric was coated by T-FAS/PDMS/SiO_2 NPs, new peaks at 800 cm^{-1} occurred, assigned to the Si-O-Si stretching vibrations. Besides, the peaks at 1210 cm^{-1}, corresponded to $-CF_2$ groups, were visible. The introduction of typical peaks can be verified by FTIR spectra of Fabric @PDMS and @T-FAS as described in Fig. S5a. The introduction of T-FAS/PDMS/SiO_2 which indicates the formation of C-F and Si-O-Si bonds on the coating surface contribute to the lower surface energy.

Furthermore, the chemical composition and surface atomic concentration of Pristine Fabric and Fabric @T-FAS/PDMS/SiO_2 were characterized by XPS, as shown in Fig. 4e. The CKLL (975 eV), C1s (284 eV) and O1s (532eV) peaks can be seen clearly in the spectrum of Pristine Fabric. After introduction of T-FAS/PDMS/SiO_2 layer, the new Si (Si2s 166 eV and Si2p 103 eV) and F (FKLL 821 eV and F1s 687 eV) signals, characteristic of covalently bonded Si and F, was detected. And the reduction in the O1s peak confirmed that Pristine Fabric was covered with a layer of PDMS and T-FAS. The change in detail can be observed in Fabric @PDMS and @T-FAS, respectively (Fig. S5b). The Si and F content sharply were enhanced to 3.6 and 46.1%, while the C and O percentage decreased to18.2 and 32.1%, respectively. High-resolution XPS provides additional insight into the chemical composition of the film further. The spectra were deconvoluted into five component peaks according to binding energies characteristic of the molecular units including C-C, C-Si, C-N, C-O and C-F as shown in Fig. S5c. Therefore, Fabric @T-FAS/PDMS/SiO_2 not only possesses enhanced roughness but also provides the fabric with low surface energy which endows fabrics with stable super-repellence.

3.5. Chemical etching and self-healing property

The chemical etching and self-healing were assessed by immersing the samples in strong acid (H_2SO_4, pH = 1) and base solutions (KOH, pH = 14) at room temperature for 12 h. The WCA

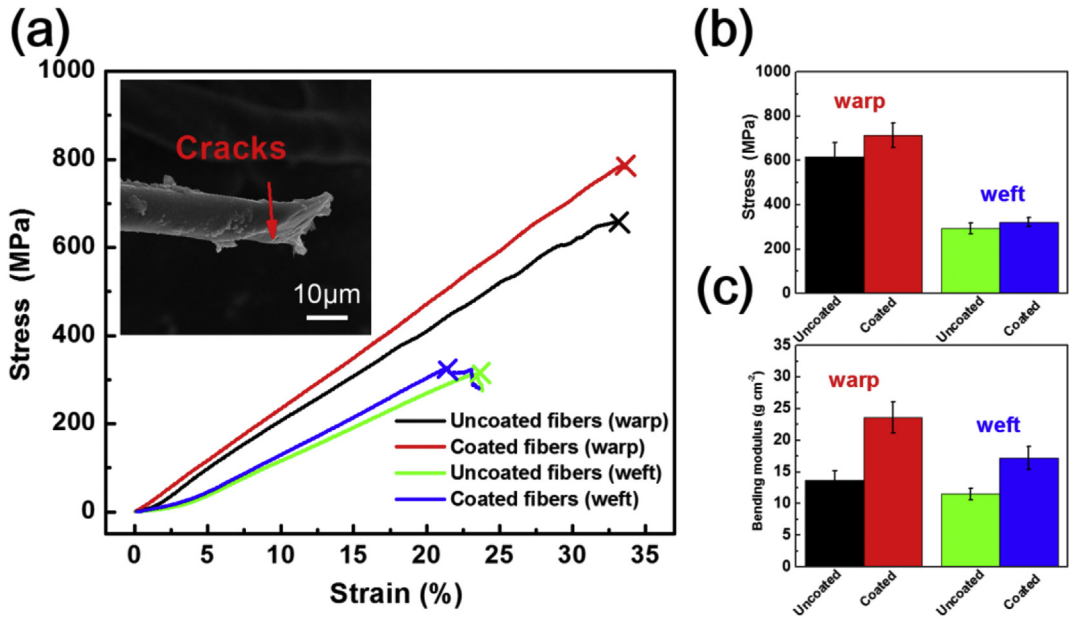

Fig. 3. (a) Stress-strain curves of fibers before and after coated, SEM images of fractured fibers (inset), (b) stress values at break in the warp and weft, respectively, before and after coated, (c) bending modulus values at break in the warp and weft, respectively, before and after coated.

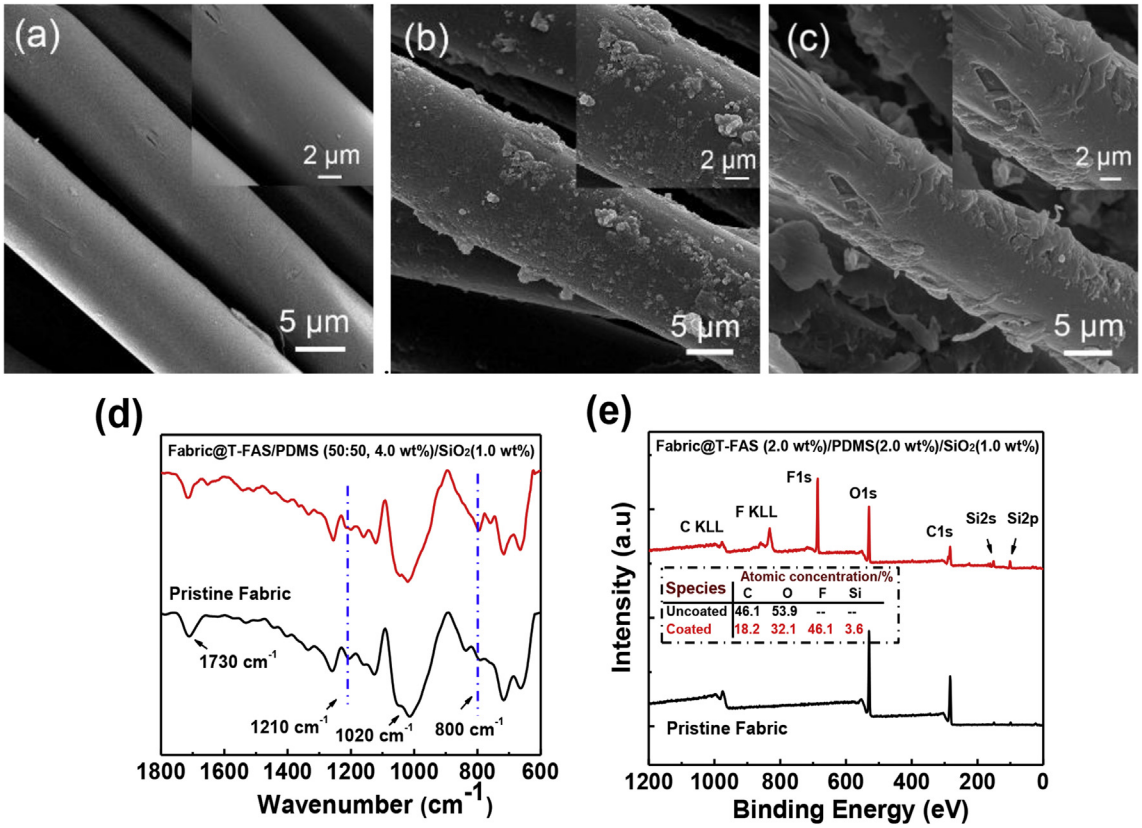

Fig. 4. SEM images of fiber (a) uncoated, (b) undamaged @T-FAS/PDMS/SiO_2, (c) damaged @T-FAS/PDMS/SiO_2, (d) FTIR spectra of Pristine Fabric, @T-FAS/PDMS/SiO_2, (e) XPS spectra of Pristine Fabric, @T-FAS/PDMS/SiO_2.

was measured after the coated fabric was rinsed with water and dried at room temperature. Fig. 5a shows the WCA values stable in strong acid while reduced in strong base solutions. There are almost no change in WCA in strong acid. When strong sulfuric acid (pH = 1) was poured onto fabric samples, the liquids rolled off completely from the coated fabric surface (Movie S3). Given that the coated fabric contains a large amount of Si-O bonds, the WCA reduced from 165° to 103° after immersed in an aqueous KOH

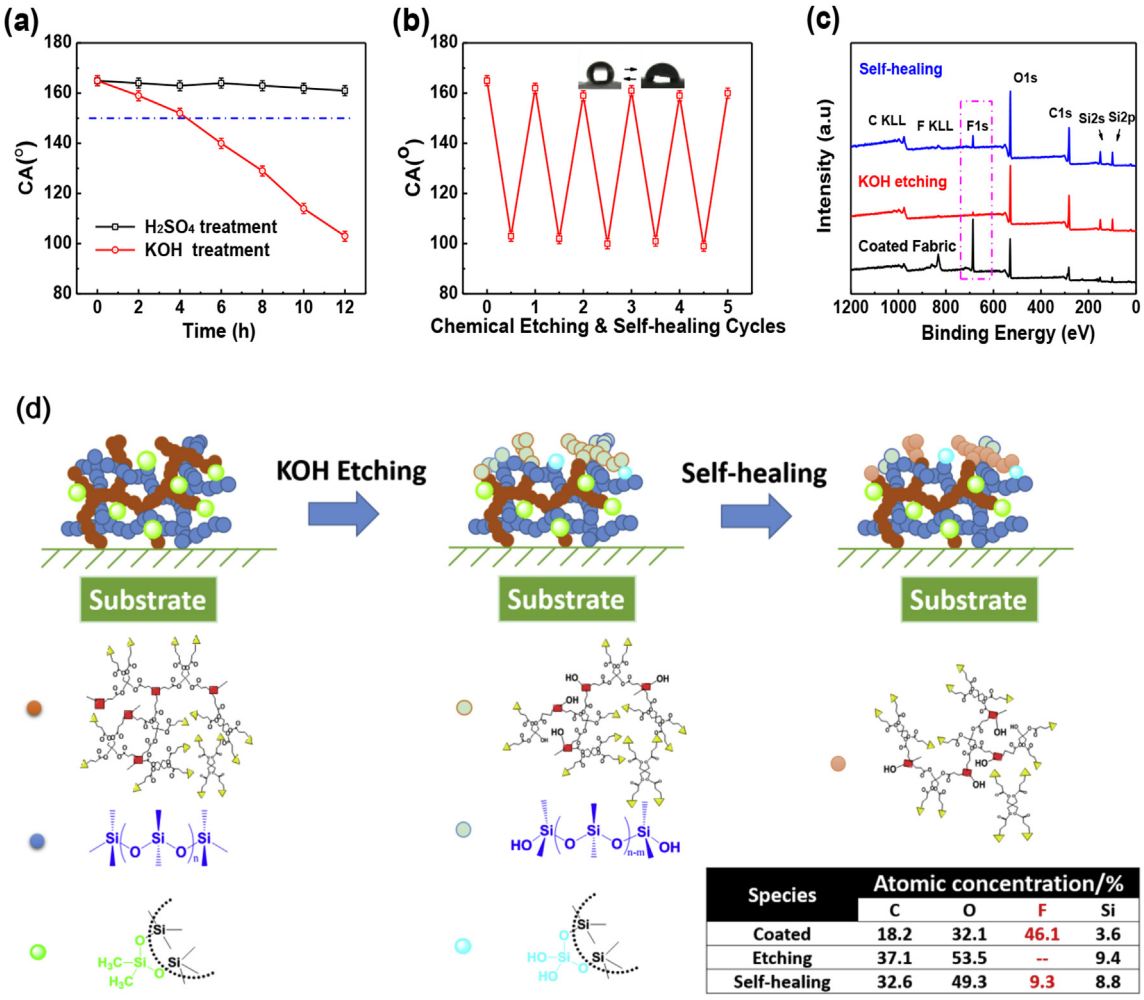

Species	Atomic concentration/%			
	C	O	F	Si
Coated	18.2	32.1	46.1	3.6
Etching	37.1	53.5	--	9.4
Self-healing	32.6	49.3	9.3	8.8

Fig. 5. (a) WCA change with time in strong acid (H_2SO_4, pH = 1) and base solutions (KOH, pH = 14) at room temperature, (b) WCA change in 5 cycles of KOH etching and heating treatment (all coated fabrics were dried at 150 °C for 1 h), (c) XPS spectra of Coated Fabric, after KOH-etching and self-healing, (d) Schematic illustration of self-healing mechanism for T-FAS/PDMS/SiO_2 coating layer and the changes of atomic concentration during coated, etching and self-healing treatment.

solution (pH = 14) for 12 h (Fig. 5a). But the KOH etched fabric was rinsed with water and heated at 150 °C for 1 h, the WCA returned to 160°, similar to its original super-repellent state (Fig. 5b). Such self-healing action could be repeated several times.

Supplementary video related to this article can be found at http://dx.doi.org/10.1016/j.compscitech.2016.10.023.

The mechanisms for self-healing of coatings should be derived from polymer chain interdiffusion, having been reported by a few groups [46,47]. Fig. 5c illustrates the steps for self-healing. The long perfluoro-terminated chains of T-FAS with adequate mobility were connected to the network as arms. When the top chains were damaged, the fluorinated chains beneath the damaged surface migrate and reorient towards the new air interface, to minimize the surface free energy. This surface replenishment repairs the super-hydrophobic system. The overall covering of long perfluoro-terminated chains of T-FAS maintains self-healing recyclable and the migration of chains can be accelerated by heating, which increases the self-healing speed.

XPS and SEM were used to confirm the mechanisms of self-healing principles. The surface chemical components and surface atomic concentration of coated Fabric, after KOH etching and self-healing were characterized as shown in Fig. 5c and d. After 12 h of KOH-etching, The F content almost reduced from 46.1 to 0%, while the O percentage is enhanced from 32.1 to 53.5%. The coatings becomes hydrophilic and the top chains damaged. By just self-healing, the fluorinated chains beneath the damaged surface migrate and the F content distinctly increases from 0 to 9.3%. Besides, SEM images showed little change after etching and self-healing treatment (Fig. S6). It verifies that the mechanisms for self-healing of coatings should be derived from polymer chain interdiffusion not molecular migration.

3.6. UV, thermal and anti-smudge durability

The samples were exposed to UV light at room temperature to assess the UV-durability of the modified coatings, and the wetting behaviors were recorded every 6 h. The static contact angle and shedding angle curves are presented in Fig. 6a. As shown, after irradiation for 48 h, the surface still exhibited a contact angle of 162 ± 2° and a shedding angle of 5 ± 1°, suggesting a superior UV-durability (Fig. S7). This can be ascribed to a large number of C-F bonds and Si-O bonds which cannot be broken by the UV light (314–419 kJ mol^{-1}).

The coated fabrics were selected to carry out thermal durability test in an air-circulating oven at 150 °C for 24 h. The influence of aging time on WCA and WSA was investigated. The coated fabrics showed almost no change in WCA and WSA as shown in Fig. 6b. Moreover, the fabrics were protected by the liquid-repellent

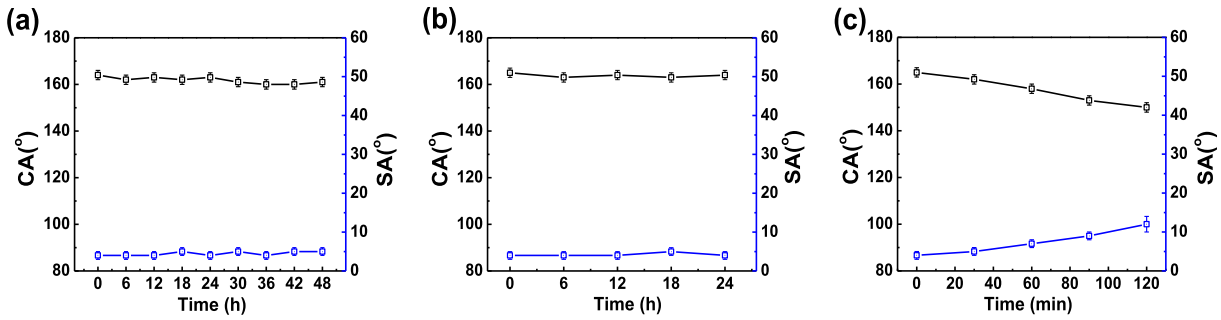

Fig. 6. (a) The effect of UV irradiation time on WCA and WSA change, (b) WCA and WSA change with time in an air-circulating oven at 150 °C, (c) WCA and WSA of the coated fabric changing with immersion time in coffee liquid.

coatings to resist yellowing. By comparation, the pristine fabrics were oxidized to a great extent (Fig. S8).

The fabrics immersed in Maxwell coffee liquid have been used to evaluate anti-smudge durability. After immersed in Maxwell coffee liquid for 2 h, followed by rinsing with water and finally dried, the coated fabric was less stained than the pristine fabrics, as shown in Fig. S9. Fig. 6c shows WCA, WSA changes with the staining time. The coating, though stain was absorbed, remains above 150° in WCA against contaminant in the liquids, being stable against contaminant in the liquids. However, for uncoated fabric after the treatment under the same condition, the fibers were seriously stained.

4. Conclusion

In summary, we developed a superhydrophobic interpenetrating polymer network that consists of a novel branched T-FAS, PDMS and SiO_2 NPs with self-healing properties. The novel branched T-FAS using an average of two long hydrolysable silane and fluoroalkyl chains, respectively as body and arms, provides highly durable and self-healing superhydrophobicity. Such robust, self-healing, superhydrophobic coatings from T-FAS and PDMS may be useful for the development of robust protective coatings for various applications.

Author contributions

The manuscript was written through contributions of all authors. All authors have given approval to the final version of the manuscript.

Notes

The authors declare no competing financial interest.

Acknowledgment

We gratefully appreciate the support of the National High Technology Research and Development Program of China (863 Program) (Grant 2012AA02A404), the Key Program of the National Natural Science Foundation of China (Grant No. 51433008) and the General Program of the National Natural Science Foundation of China (Grant No. 51173146).

Appendix A. Supplementary data

Supplementary data related to this article can be found at http://dx.doi.org/10.1016/j.compscitech.2016.10.023.

References

[1] H. Bellanger, T. Darmanin, E. Taffin de Givenchy, F. Guittard, Chemical and physical pathways for the preparation of superoleophobic surfaces and related wetting theories, Chem. Rev. 114 (5) (2014) 2694–2716.
[2] S. Wang, K. Liu, X. Yao, L. Jiang, Bioinspired surfaces with superwettability: new insight on theory, design, and applications, Chem. Rev. 115 (16) (2015) 8230–8293.
[3] T. Darmanin, F. Guittard, Recent advances in the potential applications of bioinspired superhydrophobic materials, J. Mater. Chem. A 2 (39) (2014) 16319–16359.
[4] Y. Lai, Y. Tang, J. Gong, D. Gong, L. Chi, C. Lin, Z. Chen, Transparent superhydrophobic/superhydrophilic TiO_2-based coatings for self-cleaning and anti-fogging, J. Mater. Chem. 22 (15) (2012) 7420–7426.
[5] J. Lv, Y. Song, L. Jiang, J. Wang, Bio-inspired strategies for anti-icing, ACS Nano 8 (4) (2014) 3152–3169.
[6] G.S. Watson, D.W. Green, L. Schwarzkopf, X. Li, B.W. Cribb, S. Myhra, J.A. Watson, A gecko skin micro/nano structure-A low adhesion, superhydrophobic, anti-wetting, self-cleaning, biocompatible, antibacterial surface, Acta Biomater. 21 (2015) 109–122.
[7] J.C. Brennan, N.R. Geraldi, R.H. Morris, D.J. Fairhurst, G. McHale, M.I. Newton, Flexible conformable hydrophobized surfaces for turbulent flow drag reduction, Sci. Rep. 5 (2015).
[8] A.K. Sasmal, C. Mondal, A.K. Sinha, S.S. Gauri, J. Pal, T. Aditya, M. Ganguly, S. Dey, T. Pal, Fabrication of superhydrophobic copper surface on various substrates for roll-off, self-cleaning, and water/oil separation, ACS Appl. Mater. Interfaces 6 (24) (2014) 22034–22043.
[9] J. Gu, N. Li, L. Tian, Z. Lv, C. Liang, Q. Zhang, High thermal conductivity graphite nanoplatelet/UHMWPE nanocomposites, RSC Adv. 5 (46) (2015) 36334–36339.
[10] S.K. Hong, G. Lim, S.J. Cho, Breathability enhancement of electrospun microfibrous polyurethane membranes through pore size control for outdoor sportswear fabric, Sens. Mater. 27 (1) (2015) 77–85.
[11] H.B. Yao, H.Y. Fang, X.H. Wang, S.H. Yu, Hierarchical assembly of micro-/nano-building blocks: bio-inspired rigid structural functional materials, Chem. Soc. Rev. 40 (7) (2011) 3764–3785.
[12] S. Nagappan, C.-S. Ha, Emerging trends in superhydrophobic surface based magnetic materials: fabrications and their potential applications, J. Mater. Chem. A 3 (7) (2015) 3224–3251.
[13] R. Liao, Z. Zuo, C. Guo, Y. Yuan, A. Zhuang, Fabrication of superhydrophobic surface on aluminum by continuous chemical etching and its anti-icing property, Appl. Surf. Sci. 317 (2014) 701–709.
[14] L. Li, V. Breedveld, D.W. Hess, Design and fabrication of superamphiphobic paper surfaces, ACS Appl. Mater. Interfaces 5 (11) (2013) 5381–5386.
[15] Y. Li, J. John, K. Carter, Superhydrophobic coating sheets made by roll-to-roll nanoimprint lithography, Adv. Funct. Mater. (2014).
[16] Y. Liu, X. Yin, J. Zhang, S. Yu, Z. Han, L. Ren, A electro-deposition process for fabrication of biomimetic super-hydrophobic surface and its corrosion resistance on magnesium alloy, Electrochim. Acta 125 (2014) 395–403.
[17] C.R. Crick, J.C. Bear, A. Kafizas, I.P. Parkin, Superhydrophobic photocatalytic surfaces through direct incorporation of titania nanoparticles into a polymer matrix by aerosol assisted chemical vapor deposition, Adv. Mater. 24 (26) (2012) 3505–3508.
[18] S. Zhai, E.-J. Hu, Y.-Y. Zhi, Q. Shen, Fabrication of highly ordered porous superhydrophobic polystyrene films by electric breath figure and surface chemical modification, Colloid Surf. A physicochem. Eng. Asp. 469 (2015) 294–299.
[19] X. Tang, Y. Si, J. Ge, B. Ding, L. Liu, G. Zheng, W. Luo, J. Yu, In situ polymerized superhydrophobic and superoleophilic nanofibrous membranes for gravity driven oil-water separation, Nanoscale 5 (23) (2013) 11657–11664.
[20] X. Fan, X. Jia, H. Zhang, B. Zhang, C. Li, Q. Zhang, Synthesis of raspberry-like poly (styrene-glycidyl methacrylate) particles via a one-step soap-free emulsion polymerization process accompanied by phase separation, Langmuir 29 (37) (2013) 11730–11741.

[21] X. Deng, L. Mammen, H.-J. Butt, D. Vollmer, Candle soot as a template for a transparent robust superamphiphobic coating, Science 335 (6064) (2012) 67–70.
[22] L. Gao, S. Xiao, W. Gan, X. Zhan, J. Li, Durable superamphiphobic wood surfaces from Cu_2O film modified with fluorinated alkyl silane, RSC Adv. 5 (119) (2015) 98203–98208.
[23] L. Shen, W. Qiu, W. Wang, G. Xiao, Q. Guo, Facile fabrication of superhydrophobic conductive graphite nanoplatelet/vapor-grown carbon fiber/polypropylene composite coatings, Compos. Sci. Technol. 117 (2015) 39–45.
[24] T. Verho, C. Bower, P. Andrew, S. Franssila, O. Ikkala, R.H. Ras, Mechanically durable superhydrophobic surfaces, Adv. Mater 23 (5) (2011) 673–678.
[25] C. Xue, J. Ma, Long-lived superhydrophobic surfaces, J. Mater. Chem. A 1 (13) (2013) 4146.
[26] D.S. Facio, M.J. Mosquera, Simple strategy for producing superhydrophobic nanocomposite coatings in situ on a building substrate, ACS Appl. Mater. Interfaces 5 (15) (2013) 7517–7526.
[27] H. Zou, S. Lin, Y. Tu, G. Liu, J. Hu, F. Li, L. Miao, G. Zhang, H. Luo, F. Liu, Simple approach towards fabrication of highly durable and robust superhydrophobic cotton fabric from functional diblock copolymer, J. Mater. Chem. A 1 (37) (2013) 11246–11260.
[28] Y. Zhao, Z. Xu, X. Wang, T. Lin, Photoreactive azido-containing silica nanoparticle/polycation multilayers: durable superhydrophobic coating on cotton fabrics, Langmuir 28 (15) (2012) 6328–6335.
[29] X.J. Ye, Y.X. Song, Y. Zhu, G.C. Yang, M.Z. Rong, M.Q. Zhang, Self-healing epoxy with ultrafast and heat-resistant healing system processable at elevated temperature, Compos. Sci. Technol. 104 (2014) 40–46.
[30] Y. Li, L. Li, J. Sun, Bioinspired self-healing superhydrophobic coatings, Angew. Chem. Int. Ed. 122 (35) (2010) 6265–6269.
[31] J. Gu, X. Yang, C. Li, K. Kou, Synthesis of cyanate ester microcapsules via solvent evaporation technique and its application in epoxy resins as a healing agent, Eng. Chem. Res. 55 (41) (2016) 10941–10946.
[32] Z. Wu, H. Wang, M. Xue, X. Tian, X. Ye, H. Zhou, Z. Cui, Facile preparation of superhydrophobic surfaces with enhanced releasing negative air ions by a simple spraying method, Compos. Sci. Technol. 94 (2014) 111–116.
[33] Y. Li, B. Ge, X. Men, Z. Zhang, Q. Xue, A facile and fast approach to mechanically stable and rapid self-healing waterproof fabrics, Compos. Sci. Technol. 125 (2016) 55–61.
[34] T.T. Isimjan, T. Wang, S. Rohani, A novel method to prepare superhydrophobic, UV resistance and anti-corrosion steel surface, Chem. Eng. J. 210 (2012) 182–187.
[35] J. Gu, C. Liang, J. Dang, W. Dong, Q. Zhang, Ideal dielectric thermally conductive bismaleimide nanocomposites filled with polyhedral oligomeric silsesquioxane functionalized nanosized boron nitride, RSC Adv. RSC Adv. 6 (42) (2016) 35809–35814.
[36] H. Zhou, H. Wang, H. Niu, A. Gestos, X. Wang, T. Lin, Fluoroalkyl silane modified silicone rubber/nanoparticle composite: a super durable, robust superhydrophobic fabric coating, Adv. Mater. 24 (18) (2012) 2409–2412.
[37] H. Wang, H. Zhou, A. Gestos, J. Fang, T. Lin, Robust, superamphiphobic fabric with multiple self-healing ability against both physical and chemical damages, ACS Appl. Mater. Interfaces 5 (20) (2013) 10221–10226.
[38] C.-H. Xue, X.-J. Guo, M.-M. Zhang, J.-Z. Ma, S.-T. Jia, Fabrication of robust superhydrophobic surfaces by modification of chemically roughened fibers via thiol–ene click chemistry, J. Mater. Chem. A 3 (43) (2015) 21797–21804.
[39] W.J. Yang, X. Tao, T. Zhao, L. Weng, E.-T. Kang, L. Wang, Antifouling and antibacterial hydrogel coatings with self-healing properties based on a dynamic disulfide exchange reaction, Polym. Chem. 6 (39) (2015) 7027–7035.
[40] L. Xiong, L.L. Kendrick, H. Heusser, J.C. Webb, B.J. Sparks, J.T. Goetz, W. Guo, C.M. Stafford, M.D. Blanton, S. Nazarenko, D.L. Patton, Spray-deposition and photopolymerization of organic-inorganic thiol-ene resins for fabrication of superamphiphobic surfaces, ACS Appl. Mater. Interfaces 6 (13) (2014) 10763–10774.
[41] C.E. Hoyle, A.B. Lowe, C.N. Bowman, Thiol-click chemistry: a multifaceted toolbox for small molecule and polymer synthesis, Chem. Soc. Rev. 39 (4) (2010) 1355–1387.
[42] L.C. Hu, K.J. Shea, Organo-silica hybrid functional nanomaterials: how do organic bridging groups and silsesquioxane moieties work hand-in-hand, Chem. Soc. Rev. 40 (2) (2011) 688–695.
[43] J. Shin, S. Nazarenko, C.E. Hoyle, Effects of chemical modification of thiol-ene networks on enthalpy relaxation, Macromolecules 42 (17) (2009) 6549–6557.
[44] J. Zimmermann, S. Seeger, F.A. Reifler, Water shedding angle: a new technique to evaluate the water-repellent properties of superhydrophobic surfaces, Text. Res. J. 79 (17) (2009) 1565–1570.
[45] K. Liu, X. Yao, L. Jiang, Recent developments in bio-inspired special wettability, Chem. Soc. Rev. 39 (8) (2010) 3240–3255.
[46] T. Dikic, W. Ming, R.A. van Benthem, A.C. Esteves, G. de With, Self-replenishing surfaces, Adv. Mater. 24 (27) (2012) 3701–3704.
[47] M. Yamaguchi, S. Ono, M. Terano, Self-repairing property of polymer network with dangling chains, Mater. Lett. 61 (6) (2007) 1396–1399.